metals

MDPI

Review

Electron-Beam Surface Treatment of Metals and Alloys: Techniques and Trends

Stefan Valkov *, Maria Ormanova and Peter Petrov *

Institute of Electronics, Bulgarian Academy of Sciences, 72 Tzarigradsko Chaussee blvd., 1784 Sofia, Bulgaria; m.ormanova@ie.bas.bg

* Correspondence: stsvalkov@gmail.com (S.V.); pipetrov@ie.bas.bg (P.P.); Tel.: +359-2-979-59-14 (S.V.); +359-2-797-56-78 (P.P.)

Received: 21 July 2020; Accepted: 8 September 2020; Published: 10 September 2020

Abstract: During the last decades, electron-beam treatment technologies (EBTT) have been widely used for surface modification of metals and alloys. The EBT methods are known as accurate and efficient. They have many advantages in comparison with the conventional techniques, such as very short technological process time, uniform distribution of the energy of the electron beam, which allows a precise control of the beam parameters and formed structure and properties of the materials, etc. Moreover, electron-beam treatment technologies are a part of the additive techniques, which are known as modern methods for manufacturing of new materials with unique functional properties. Currently, modern trends in the surface treatment of metals and alloys are based on the combination of electron-beam technologies with other methods, such as thin film deposition, plasma nitriding, etc. This approach results in a significant improvement in the surface properties of the materials which opens new potential applications and can involve them into new industrial fields. This paper aims to summarize the topics related to the manufacturing and surface treatment of metals and alloys by means of electron-beam technologies. Based on a literature review, the development and growth of EBT are considered in details. The benefits of these technologies—as well as their combination with other methods—are extensively discussed.

Keywords: electron-beam treatment; metals and alloys; hybrid techniques; titanium alloys; aluminum alloys; tool steels; stainless steels

1. Introduction

Due to the reduction of natural resources and continuous growth of the modern industry, the involvement of new technologies for the manufacturing of materials, as well as for modification of their structure and properties is of major importance. Currently, the electron-beam treatment methods receive much attention and are already successfully introduced in many industrial branches, such as aircraft and automotive industries, for the manufacturing of space ships, railway cars, etc. [1–6]. At these techniques, the materials are treated by a high-intensity electron beam. The kinetic energy of the electrons is transferred into heat, leading to a formation of thermal distribution from the surface to the bulk [7–9]. The heating and cooling rates are quite high which results in changes in the microstructure, chemical composition, melting the surface, etc. The technological conditions can be precisely controlled, which allows precise control of the structure and properties of the treated materials [9,10]. Some advantages of EBTT in comparison with conventional methods can be drawn as follows:

- Significantly low cost in comparison with traditional technologies;
- Significantly shorter process time in comparison with traditional technologies;

- Uniform distribution of the energy of the electron beam;
- The technological conditions defined by the technological parameters are highly reproducible.

EBTT for surface modification of metals and alloys can be used in different types of techniques:

- Electron-beam surface hardening;
- Combined methods for a surface hardening;
- Electron-beam alloying;
- Electron-beam evaporation and deposition.

When the temperature on the surface of the workpiece reaches a value lower than the melting point of the material, the treated zone remains in solid–state, but some structural changes and phase transformations occur. This method can be used mostly for hardening [5]. In the case of reaching the melting point of the specimen, the treated surface area becomes in liquid–state where some alloying elements can be introduced. This technique is used for surface alloying, welding, hardening and texturing processes [5]. In addition, the EBTT can be used for evaporation and thin-film deposition when the obtained surface temperature reaches the point where a significant amount is evaporated (or sublimated) [11].

This paper aims to summarize the topics of electron-beam surface treatment of new functional materials and we present and discuss the techniques and trends of improvement of their structure and properties. Significant attention is paid to the combined methods, where electron-beam treatment is combined with other methods, such as plasma nitriding, thin film deposition, etc.

2. Electron-Beam Surface Treatment: Heat Processes

There exist two types of electron-beam surface treatment technologies, namely continuous and pulsed. Both techniques significantly differ from each other, where the main difference is the heating and cooling rate. In the case of pulsed EBT, this rate can reach values of 10^9 K/s [12,13], while in the continuous mode it is about 10^5 K/s [14], which leads to the different structure and functional properties of the processed materials. In both types of techniques, the energy parameters of the beam are of major importance and are as follows: The acceleration voltage U [V]; the beam current I [A] and the beam diameter d [15]. The input energy density can be defined as follows:

$$E = \frac{UIt}{S} \quad (1)$$

In (1) E—Input energy density [J/mm^2]; t—irradiation time [s]; S—Irradiated area [mm^2].

The experimental types of equipment available in the scientific laboratories, as well as in factories for commercial manufacturing is based on the use of a high-intensity electron beam, which is generated by an electron gun. A scheme of typical electron-beam equipment with the continuous mode is shown in Figure 1. The emitted from the cathode electrons are accelerated by accelerating voltage and are stacked into a beam with a conical shape by accelerating and focusing electric fields. After this, it passes through the system of focusing lens and deflecting coils, where the electrons are deflected electromagnetically and are guided on the surface of the treated specimen [16,17].

Considering the continuous-wave process, the treatment is realized by scanning the surface, where the sample is moving under the electron beam with a constant velocity. At this experiment, the electrons can be deflected from the normal axis and different scanning trajectory of the electron beam can be realized (Figure 2). This allows precise control of the cooling rate and lifetime of the melt pool, and, therefore of the resultant structure and properties of the material. For example, using the linear manner of scanning (i.e., dithering, Figure 2a), the cooling rate is significantly higher in comparison with the circular one (Figure 2b). The use of circular geometry of scanning leads to a longer lifetime of the melt pool due to the overlap of the beam trajectory (Figure 3a,b) [18]. As a result, the distribution of the alloying elements within the alloyed zone is much more homogeneous [19].

The use of more complex scanning figures (Figure 2d–h) leads to a redistribution of the kinetic energy of the electrons, and therefore, to a transformation in the thermal field generated in the workpiece. This could lead to a change in the fluid flow dynamic processes, to a formation of additional streams, responsible for the distribution and homogenization of the alloying elements and different lifetime of the melt pool. All these features are of major importance for the resultant functional properties of the processed materials. The electron-beam scanning frequency and speed of the specimen motion during the treatment process are also important parameters because they are directly linked to the irradiation time, defined in Formula (1), as well as for the cooling rate and solidification speed. Considering the pulsed-wave technique, in addition to the accelerating voltage, beam current and beam diameter, the pulse duration (τ) is also of major importance. Most of these experiments are designed as follows: the specimen is irradiated by a high-intensity pulsed electron beam and higher values of τ lead to higher irradiation time and input energy density, respectively [13].

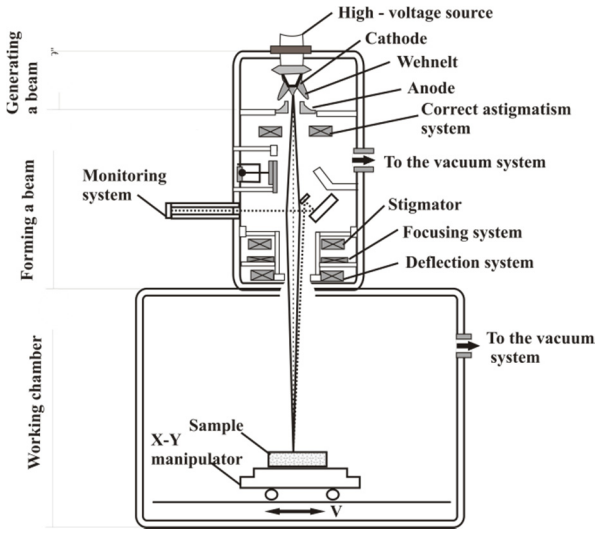

Figure 1. Scheme of electron-beam equipment for surface modification.

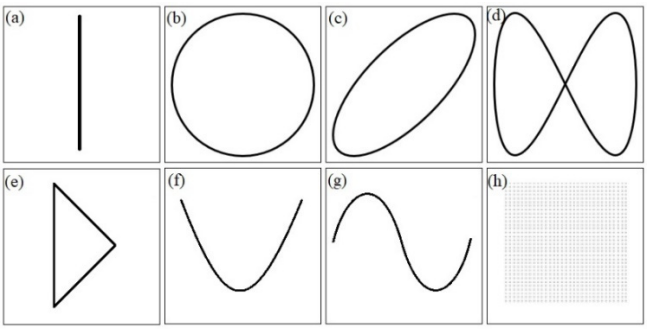

Figure 2. Electron-beam scanning figures. (**a**) Line; (**b**) circle; (**c**) ellipse; (**d**) infinity; (**e**) triangle; (**f**) parable; (**g**) sine; (**h**) matrix.

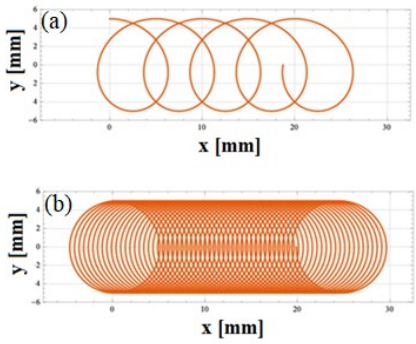

Figure 3. Example of circle electron-beam scanning figure at (**a**) low scanning frequency and (**b**) high scanning frequency [18]. (Reproduced with permission from ref. [18]. Copyright (2019), Elsevier).

As already mentioned, at electron-beam processing of materials, the kinetic energy of the electrons is transferred into heat, which leads to a formation of thermal distribution from the surface to the bulk [20]. Figure 4 schematically presents the processes of electron-beam interaction with materials. However, not all electrons penetrate and release their energy into the material. Some of the incident electrons lose their energy in other forms: reflected electrons, heat radiation, secondary electrons or X-rays, as shown in Figure 4.

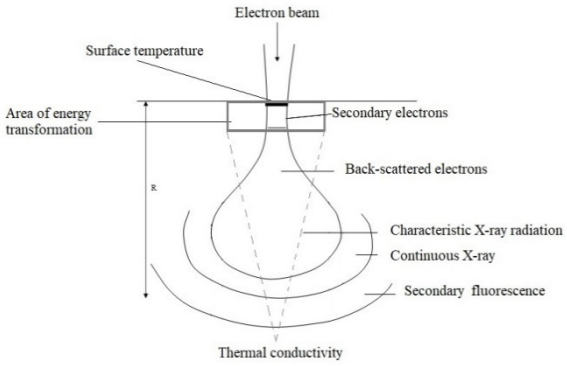

Figure 4. Scheme of electron-beam interaction with materials.

In the case of electron-beam surface treatment and modification, very high heating and cooling rates exist, leading to changes in the microstructure, phase composition, improvement of the functional properties, etc. Therefore, the correct assessment of the thermal field within the sample during the EBTT process is of major importance. There exist both, experimental and numeric approaches of evaluation of the thermal distribution. The numeric methods are widely used for this purpose and are significantly more appropriate in comparison with the experiments because the latter techniques are consuming significant time and effort. Moreover, the results are not always reliable. For electron-beam treatment of homogeneous and isotropic material with temperature-independent physical properties, the heat transfer equation can be written in the following form [21,22]:

$$\frac{1}{\alpha}\frac{\partial T}{\partial t} - \nabla^2 T = \frac{f(r,t)}{\lambda} \tag{2}$$

In (2): α—thermal diffusivity ($\alpha = \frac{\lambda}{c\rho}$); λ—thermal conductivity; c—specific heat; ρ—density of the material. In this case the heat distribution of the electron beam is related to that of the heat source

$f(r,t)$ at location r and time t. The solution of Equation (1) can be expressed by three dimensional Green's function and is given as follows [23]:

$$\mathrm{T(r,t)} = \frac{\alpha}{\lambda}\int_{\tau=0}^{t} d\tau \int_{R} G(r,t|r',\tau)f(r',\tau)dV' + \int_{R} G(r,t\left|r',\tau\right)|_{\tau=0}F(r')dV' \tag{3}$$

In Equation (3), $F(r')$ corresponds to the initial temperature distribution. The physical interpretation of the Green's function $G(r,t|r',\tau)$ for three-dimensional problems is the temperature at a moment t and location r caused by a point source located at r' and its energy is released for time $t = \tau$. The "r',τ" part of the argument means the effect (i.e., the temperature in the medium located at r and moment t), the "r',τ" presents the impulse (i.e., the instantaneous point source at r' and releasing its heat for time τ). The intensity distribution of Gaussian beam, moving along a straight line can be expressed as:

$$f(x',y',\tau) = \frac{3Q}{\pi {r_0}^2} exp\left(-3\frac{(x'-v\tau)^2 + y'^2}{{r_0}^2}\right) \tag{4}$$

In (4), r_0 is the radius in which the power of the beam is equal 95% of total power; Q is the transferred power; v—beam velocity along moving line. In the case of a dithering beam the intensity distribution is:

$$f_c(x',y',\tau) = \frac{3Q}{\pi r_0^2} exp\left(-3\frac{(x'-v\tau)^2 + \left(y' - \iota_{max}\cos\left(\frac{2\pi\tau}{\tau^*}\right)\right)^2}{r_0^2}\right) \tag{5}$$

In (5) l_{max} is the amplitude; τ^* represents the period for each of the cycles. For a rotating beam, the intensity is as follows:

$$f(x',y',\tau) = \frac{3Q}{\pi {r_0}^2} exp\left(-3\frac{\left(x'-v\tau - asin\left(\frac{2\pi\tau}{\tau^*}\right)\right)^2 + \left(y' - l_{max}cos\left(\frac{2\pi\tau}{\tau^*}\right)\right)^2}{{r_0}^2}\right) \tag{6}$$

In (6) a is the diameter of the rotation.

The abovementioned model was experimentally verified in the case of electron-beam treatment of Al plate using a circular manner of scanning. During the experiments, the accelerating voltage (U) was 52 kV; the electron-beam current (I) was in the range from 18 mA to 25 mA; the speed of the specimen motion (V) was from 5 mm/s to 50 mm/s; the radius of the electron-beam rotation (R) was 2.2 mm; the characteristic beam diameter (r_0) was 0.22 mm. The results for the temperature distribution are presented in Figure 5 [18]. The melting temperature of the treated material is 660 °C and is denoted with a green line. The dependence of the speed of the specimen motion on the thermal distribution is shown in Figure 5a. During the verification, the following parameters were used: accelerating voltage U = 52 kV; electron-beam current I = 25 mA; electron-beam scanning frequency f = 10 kHz; the radius of electron-beam rotation R = 2.2 mm; beam diameter r = 0.22 mm. Figure 5b shows the dependence of the power of the heat source ($Q = U{\cdot}I$) on the thermal distribution within the Al substrate. The electron-beam treatment conditions used for evaluation of the influence of the power of the heat source were defined by the following parameters: speed of the specimen motion V = 50 mm/s; electron-beam scanning frequency f = 10 kHz; the radius of electron-beam rotation R = 2.2 mm; beam diameter r = 0.22 mm. The effect of the scanning frequency is presented in Figure 5c. The technological conditions were defined by the following parameters: accelerating voltage U = 52 kV; electron-beam current I = 25 mA; the speed of the specimen motion V = 50 mm/s; the radius of electron-beam rotation R = 2.2 mm; beam diameter r = 0.22 mm. It is obvious that the electron-beam scanning frequency has the greatest influence on the thermal distribution.

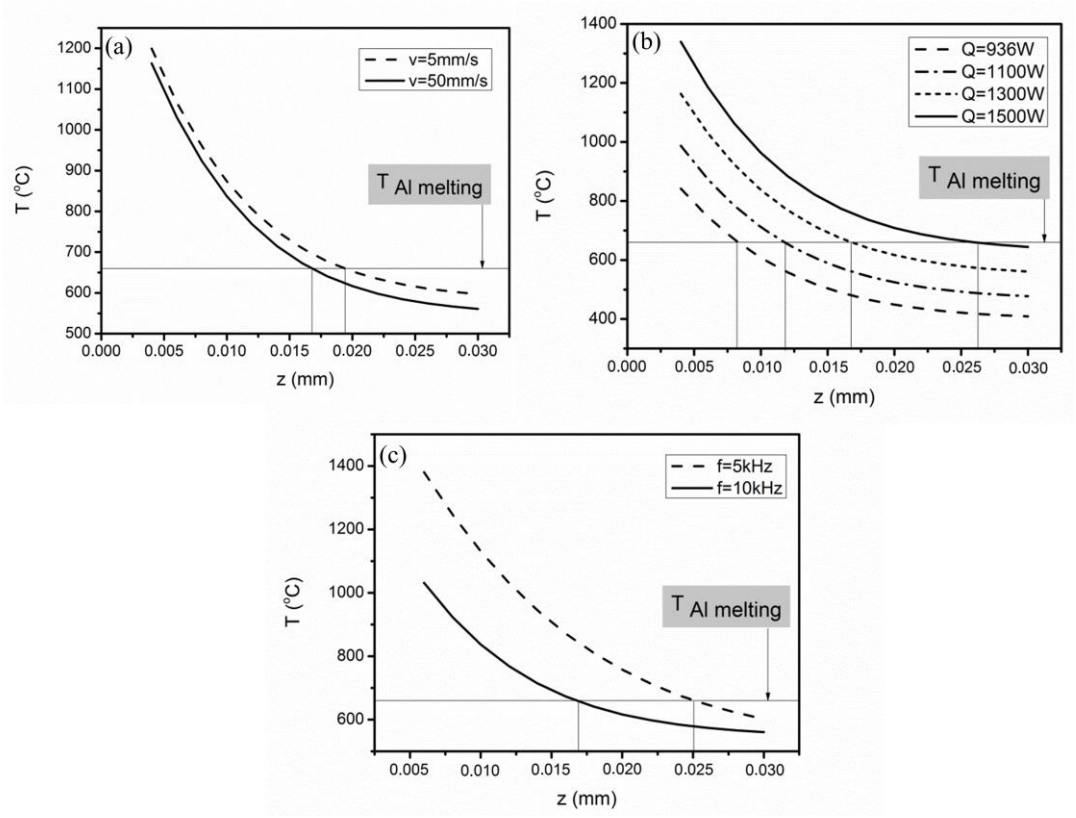

Figure 5. Distribution of the temperature along z axis for a (**a**) different velocities of specimen motion; (**b**) different electron-beam power; (**c**) different electron-beam scanning frequencies [18]. (Reproduced with permission from ref. [18]. Copyright (2019), Elsevier).

The speed of the specimen motion during the treatment process influences the temperature very weakly (Figure 5a) where the temperature decreases with only a few degrees with an increase in the velocity from 5 mm/s to 50 mm/s. In addition, an increase in the electron-beam power leads to an increase in the thickness of the treated zone. Considering the influence of the electron-beam scanning frequency on the temperature distribution (Figure 5c) of the depth of the melt pool, it decreases from 25 μm to 17 μm with a decrease in the electron-beam scanning frequency [18]. The results obtained by the authors of [18] showed a full agreement with the experimentally measured depth of the molten zone of the treated samples.

Similarly, D. Kaisheva [24] has evaluated the cooling rates of alloyed steel (0.11 wt% C; 0.27 wt% Si; 0.6 wt% Mn; 1.35 wt% Cr; 3.25 wt% Ni; ≤0.025 wt% P; ≤0.025 wt% S; Fe bal.) at electron-beam welding using the same model, and the results obtained are presented in Figure 6. During the experiments, the accelerating voltage (U) was 60 kV; the electron-beam current (I) was 50 mA; the speed of the specimen motion (V) was 5 mm/s; the characteristic beam diameter (r_0) was 0.22 mm. The experiments were realized without oscillation of the electron beam. It was chosen three distances from the center of the weld, namely y = 1 mm; y = 1.5 mm and y = 2 mm, and the temperature was investigated at depths of 6 mm and 9 mm, respectively. The results were presented vs. the temperature at each moment from the beginning of the welding process to the point where it is 400 °C. From Figure 6, it is obvious that when the temperature decreases to 400 °C, the curves related to the distance from the center of the weld completely coincide. In addition, the cooling rate decreases with distancing from the weld center [24].

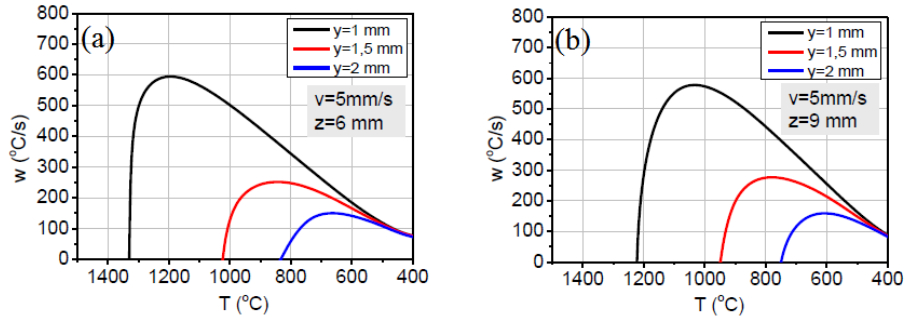

Figure 6. Cooling rates of structural steel-alloyed steel at electron-beam welding (**a**) at a depth of 6 mm; (**b**) at a depth of 9 mm.

It is obvious that the discussed above numeric model is useful for the assessment of the thermal field within the sample at the electron-beam treatment technologies. However, some limitations must be mentioned. The model does not take into account the changes of the thermo-physical characteristics (thermal diffusivity, thermal conductivity, specific heat, density of the material) of the treated materials with the changes of the temperature; the sample is considered a semi-infinite body, and its real dimensions are also not taken into account; the model has not taken into account the heat exchange between the specimen and surrounding medium.

3. Electron-Beam Surface Hardening

Electron-beam hardening is one of the most promising techniques for improvement of the surface' properties of the materials. The method is based on the heating up to a certain temperature and rapidly cooling with a very high rate, where a fine crystalline microstructure is formed. This technique allows precise heating of selected surface regions and achievement of significantly higher values in comparison with the traditional hardening methods [25]. One of the main advantages of the electron-beam hardening in comparison with the other techniques is the excellent formability and deflectability with frequencies up to 100 kHz [26].

The authors of [27] demonstrated the possibility of electron-beam surface treatment and the hardening of 5CrMoMn steel. During the experiments, the beam current was varied from 6 mA to 8 mA with a step of 0.5 mA. The results showed that the measured microhardness was 335 HV in the case of untreated material and reached values of 656 HV at a beam current of 7 mA and decreases with a further increase in the beam current due to a reduction of the carbon content and martensite. It was found that the best wear properties and the smoothest surface can be obtained at the same beam current of 7 mA [27].

Similarly, the authors of [28] studied an electron-beam surface treatment of 30CrMnSiA, where the influence of the input energy density was investigated. A cross-sectional SEM image obtained by scanning electron microscopy is shown in Figure 7. Two distinguished areas are visible, namely base metal and hardening zone. The microstructure of the base metal consists of coarse grains, while at the hardening zone, it is significantly finer, due to the very high cooling rate. A detailed analysis of the microstructure showed that the hardening zone is mostly in the form of martensite and a very small amount of bainite at the transition zone (Figure 7b).The results revealed that the microhardness increases from 320 HV for untreated material, up to 520 HV for treated steel at an input energy density of 1.875 kJ/cm^2. By further increasing the input energy density the hardness starts to decrease due to convective mixing processes of the molten material, which becomes predominant. In this area, the cooling rate is relatively low, which leads to lower values of the hardness.

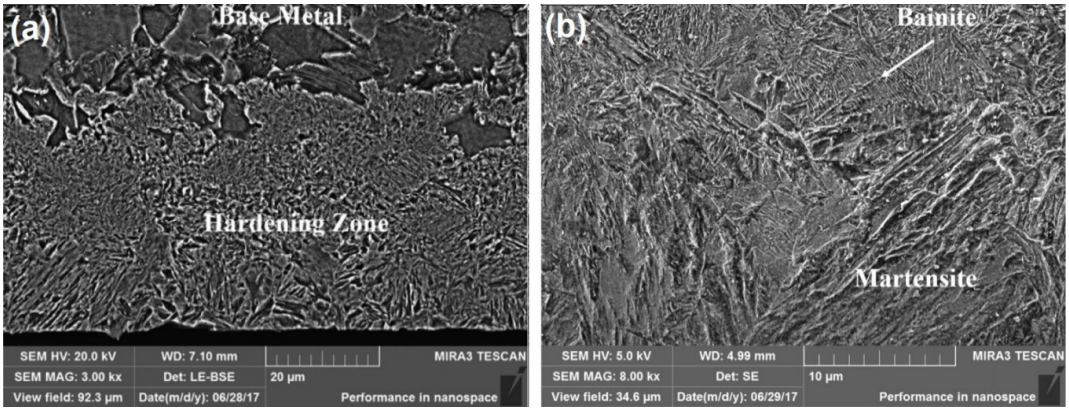

Figure 7. Cross-sectional SEM images of electron-beam-treated 30CrMnSiA steel (**a**) hardened zone; (**b**) higher magnification of the transition zone [28]. (Reproduced with permission from ref. [28]. Copyright (2017), Elsevier).

The authors of [29,30] studied an electron-beam surface hardening of 40X steel (0.36–0.44%C; 0.80–1.10%Cr; 0.50–0.80% Mn; 0.17–0.37% Si; 0.30% Ni; 0.17% Cu; 0.04% S; balance Fe). The application of the electron-beam treatment process led to a finer microstructure and an increase in the hardness due to the high heating and cooling rates. Similar results were shown in [31], where a significant increase in the hardness and wear resistance of tools and highly loaded components after the electron-beam surface treatment was observed.

Song et al. [32] studied the influence of electron-beam surface hardening on the microstructure and hardness of AISI D3 steel. The results revealed that the microstructure of the hardened zone was in the form of martensite, fine carbides and retained austenite. The transition area consisted of tempered sorbite. It was found that the microhardness was close to 1400 HV—2.5 times higher than the base material.

The titanium and its alloys are also widely used in different industrial applications, such as aircraft and automotive manufacturing, railway cars, space ships, modern medicine, dentistry, etc. These materials are characterized by their attractive mechanical properties, lightweight, excellent corrosion properties and biocompatibility. However, some drawbacks can be mentioned, such as low hardness and wear resistance and can be overcome with appropriate technology for surface manufacturing, where electron-beam surface treatment is one of the most promising methods.

In work [33] was investigated the influence of electron-beam treatment on the surface topography, microstructure and hardness of TA2 titanium alloy. The results showed that the treatment process led to a decrease in surface roughness. In addition, there were no changes in the phase composition after the electron-beam treatment process, besides the formation of dislocations. The nanohardness increases due to the presence of a significantly larger number of dislocations, as well as to the finer grains in comparison with the untreated specimen. Similarly, in work [34] an electron-beam surface modification of TA15 titanium alloys was realized. The results obtained by the author of [34] showed that the treatment process resulted in a significantly finer microstructure within the treated zone, leading to an increase in the hardness. It was found that the thickness of the treated was about 25 μm and corresponds to the hardness' gradient of the surface layer.

The authors of [35] studied an electron-beam surface modification of Ti-6Al-4V alloy. It was demonstrated that the electron-beam treatment technique serves as a method for controlling the surface topography and can be used for increasing the tribological performance on the surface of the material. The beam deflection, physical properties of the material, and the input energy were used for controlling the surface topography. No cracks, pores, and impurities were detected on the surface of the specimens. It was shown that the thickness of the melted and heat-affected zones strongly correlated with the input energy. The melted zone consisted of α'martensitic microstructure, the heat-affected exhibited

α primary (globular), α secondary (lamellar) and β phases, mixed with α′. This microstructure was formed due to the rapid cooling during the electron-beam treatment. The average microhardness of the melted and heat-affected zones was 450 ± 10 HV and 440 ± 20 HV, respectively. These values were about 22–25% greater than the base material. The increase in the microhardness was attributed to the formation of fine α′ martensitic structure. The same possibilities for controlling the surface topography and microstructure were demonstrated by the authors of [36]. The results of the study showed a surface pattering after the electron-beam treatment, due to the transformation from β to α′ martensitic.

Zagulyaev et al. [37] studied the influence of the input energy density on the microhardness and wear resistance of Al–Si alloy treated by a pulsed electron beam. The results showed that the optimal density parameters were 25, 30 and 35 J/cm^2, where the microhardness and wear properties were significantly improved.

Based on the performed literature review, it is obvious that the electron-beam treatment technologies have a large number of applications where hardened materials are required and have many benefits in comparison with the traditional methods. During the hardening procedure, the electron-beam parameters and technological conditions must be precisely optimized. The workpiece should be heated up to a temperature above transformation martensitic temperature, but at the same time lower than the melting point. As a result of the very high cooling rate, fine microstructure on the surface of the specimen, which can be characterized with significantly higher hardness in comparison with the base (untreated) material, is formed. At the same time, the electron-beam hardening of the surface of a specimen without melting leads to the same surface roughness as before procedure or very slight changes can be observed. On the other hand, melting of the surface during the electron-beam hardening, lead to a significant increase in the surface roughness. At the same time, this approach gets to much better performance characteristics, in comparison with the transformation hardening, due to the improved tribological properties and a significant increase in the microhardness [38]. Therefore, the selection and optimization of the electron-beam process parameters and technological conditions strongly depend on the purposes and requirements for the surfaces of the materials.

However, the single technique for electron-beam hardening has reached its threshold of development. Currently, many scientists have directed their efforts for developing combined techniques and methods for surface hardening, which are extensively discussed in the following section of this article.

4. Combined Methods for a Surface Hardening

The combination of several methods for a surface hardening, including electron-beam treatment (EBT), plasma nitriding (PN), thin film deposition, etc. is currently a subject of research by many investigators all over the world. The main idea of the combination of more than one technology is to combine their advantages.

Such an approach was successfully introduced by the authors of [39], where a combination of plasma nitriding and subsequent electron-beam treatment was applied on samples of 40X steel. The results showed that the hardness of the treated area was increased about 3 times in comparison with the base material. It was found that the use of this combined technique led to an increase in the abrasive wear more than two times in comparison with the specimen treated only with plasma nitriding.

The combinations of EBT + PN and PN + EBT were applied to tools and components [40]. It was found that the thickness of the treated layer after electron-beam treatment and plasma nitriding was two times larger in comparison with the case of PN. The hardness on the surface of the plasma nitrided sample was 680 HV, while in the case of PN + EBT it reached values of 800 HV. In addition, the combination of EBT + PN led to an increase in the microhardness up to 1200 HV.

Ormanova et al. [41] showed a combined method for a surface hardening of tool steel W320. The method consisted of EBT + PN and EBT + PN + EBT. The microstructure of the sample after electron-beam treatment and plasma nitriding exhibits an N-rich layer with a thickness of about 25 μm. The nitrogen atoms were incorporated into the steel, leading to a formation of Fe_3N phase and

microhardness of about 760 HV—or about four times higher than the base material. A cross-sectional SEM image of the sample obtained after the application of additional electron-beam treatment is shown in Figure 8. A gradient microstructure, consisting of a thin (about 2–3 μm) layer formed due to the interaction of the electrons with the specimen (zone A from Figure 8), followed by a diffusion structure (zone B) with a thickness of about 25 μm and the base material (zone C) was formed. The authors reported a slight decrease in the microhardness at a depth from 5 μm to 24 μm from the previous sample (i.e., electron-beam-treated, followed by plasma nitriding) due to a redistribution of the N atoms and larger grain size of the treated zone [41]. It should be noted that the discussed works [39–41] represent a significant improvement in the microhardness and can be involved in completely new directions of the modern industry. The increase in microhardness is based on the formation of Fe–N phases, which are characterized by significantly enhanced mechanical properties over the base material. Additionally, the electron-beam treatment technology leads to the formation of much finer microstructure. In this case, the grain boundaries play a role as a barrier for the movement of the dislocations. The above-mentioned articles [39–41] showed the effectiveness of the combination of plasma nitriding and electron-beam treatment, resulted in significant improvement in the mechanical properties over the base material (more than 3 times).

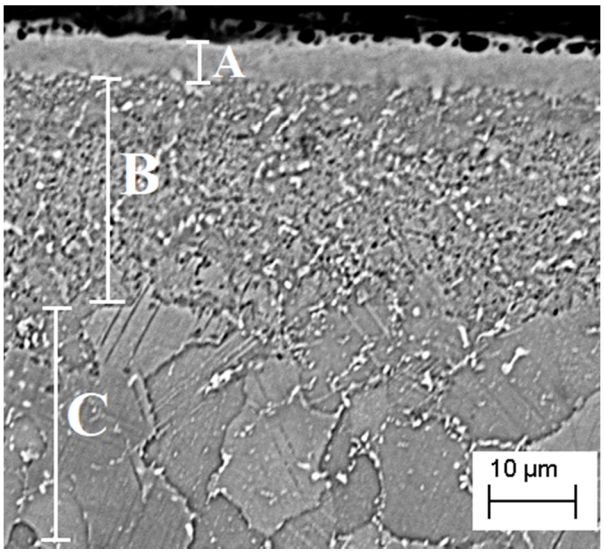

Figure 8. Cross-sectional SEM images of W320 tool steel after electron-beam treatment, plasma nitriding and subsequent electron-beam treatment [41]. (Reproduced with permission from ref. [41]. Copyright (2017), Elsevier).

In work [42] was shown a combination of EBT, PN and deposition of a CrN coating. At a combination of plasma nitriding and subsequent electron-beam treatment, a formation of a nitrogen-rich martensitic layer with a hardness of 950 HV was obtained, which was higher than the specimen treated only with plasma nitriding (750 HV). It was established that the thickness of the martensitic layer increases with an increase in the energy of the beam during the EBT. Concerning the case of EBT + PN, a nitrogen-rich layer with a hardness of about 900 HV was obtained. The combination of EBT + PN + CrN led to a further increase in the microhardness, up to about 1100 HV. In this case, the coefficient of friction of EBT + PN + CrN was lower than the EBT + PN and PN + EBT specimens. Similarly, Ormanova et al. [43] studied a surface modification of tool steel using EBT + PN and subsequent deposition of a bilayer coating of TiN/CrN. The initial surface treatment by means of a scanning electron beam, followed by plasma nitriding led to an increase in the microhardness on the surface of the substrate. In this case the difference in the mechanical properties between the substrate and the coating is significantly reduced, and a formation of internal stresses at the interface could not be expected.

Furthermore, the EBT + PN procedure is capable in improving the adhesiom between the coating and the substrate. A cross-sectional SEM image of the sample treated by EBT + PN and TiN/CrN is shown in Figure 9. The bilayer coating was deposited on a gradient microstructure, consisting of a diffusion layer with a thickness of about 5 μm, followed by significantly finer microstructure. The grains become larger towards the core of the specimen [43].

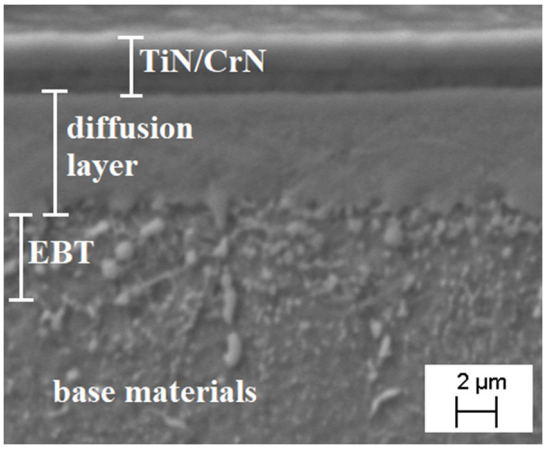

Figure 9. Cross-sectional SEM images of W320 tool steel after electron-beam treatment, plasma nitriding and a deposition of a bilayer TiN/CrN coating [43]. (Reproduced with permission from ref. [43]. Copyright (2017), Bulgarian Academy of Sciences: Union of Chemists in Bulgaria).

Petrov et al. [44] studied the effect of electron-beam treatment of Ti5Al4V alloy on the phase composition, surface topography and mechanical properties of a bilayer TiN/TiO_2 coating deposited by reactive magnetron sputtering. The results revealed that the EBT of the Ti-based alloy led to an increase in the surface roughness, from 8 nm to 25 nm and a slight decrease in the hardness, from 7 GPa to 6 GPa and reduced coefficient of friction. The same authors [44] mentioned that the increase in the surface roughness led to less colonization of the surface by bacterial cells than the conventional fabricated surfaces. Furthermore, the obtained values for the hardness after the EBT of the substrate are closer to that of the human bones and the severe stress-shielding effect after implants insertion into the body could not be expected. Similar work was carried out by Valkov et al. [45]. The authors studied the effect of electron-beam treatment of Co–Cr alloy on the growing mechanism, surface topography and mechanical properties of bilayer TiN/TiO_2 coating. The results showed that before the EBT of the base material, the growing mechanism was three-dimensional (Volmer–Weber mechanism) to two-dimensional layer-by-layer (Frank-Van-der Merwe) mechanism. In addition, the treatment process led to an increase in the surface roughness, about 3 times and a decrease in the hardness from 10 GPa to 5 GPa. The aforementioned works [44,45] demonstrated an interesting approach for controlling the surface properties of biomedical materials. The problem related to an increase in the contact area and cell-adhesion support was solved by increasing the surface roughness. Additionally, the deposition of biocompatible coatings, such as bilayer TiN/TiO_2 could open novel applications of these materials for the manufacturing of different dental and orthopedic implants, as well as for other branches of contemporary medicine.

The authors of [46] studied a combined treatment of tool steels using the deposition of a $Ti_{1-x}Al_xN$ coating, followed by electron-beam surface hardening. It was found that the coating has significantly improved the absorption properties of the base material, leading to a significant increase in the depth of the treated zone. Moreover, the depth of the hardened zone has increased with an increase in the Al content and the thickness of the Ti–Al–N coating. It was demonstrated that an electron-beam hardening of material with previously deposited film resulted in a formation of a significantly harder-treated zone than uncoated materials.

The authors of [47] demonstrated a two-stage process for surface modification of Al–11Si–2Cu alloy. The first step of the process was a deposition of multicomponent coating of Ti–Y_2O_3 by ion–plasma jet. The second stage was irradiation by a pulsed electron beam. The results showed that a multielemental layer with a thickness of 60–70 μm with a nanocrystalline structure was formed. Similarly, Zaguliaev et al. [48] studied the effect of the electron–plasma alloying process on the structure and mechanical properties of Al–Si alloy. At the experiments, alloying elements of Al and Y_2O_3 were deposited on the base material and the samples were treated by a pulsed electron beam. The results showed that a nanocrystalline layer with a thickness of 70 μm and significantly improved wear properties and higher microhardness was formed.

The combined methods are currently the latest step in the development of the techniques for surface manufacturing, which are based on electron-beam treatment. Many researchers are currently working on the formation of improved surface properties of many materials by combining EBTT with other techniques, such as plasma nitriding, thin film deposition, etc. These methods are extensively used for needs and purposes, where significantly improved mechanical properties on the surface of the materials are required. At the same time, the combined methods can be successfully used for surface treatment of materials for biomedical applications. It can be summarized that, at the moment, the combination of more than one method for surface treatment is a leading technology and the number of researchers that are based their investigations on this thematic rapidly grows. The combined methods are very promising, and the effort of many scientists is directed to the further growth of these technologies.

5. Electron-Beam Alloying

This process allows a formation of surface alloys and coatings with significantly improved functional properties than the base material (substrate). The energy of the electrons is absorbed and transferred to the lattice and the treated zone rapidly reaches the melting point of the material, forming a melt pool. The alloying elements are incorporated and distributed within the molten material and after the solidification a surface alloy with significantly enhanced functional properties over the base material is formed.

5.1. Electron-Beam Surface Alloying of Aluminum and Its Alloys

A number of studies exist describing an electron-beam surface alloying of Al and aluminum alloys [49–57]. The authors of [50–52] have studied the formation and characterization of Al–Si and Al–C surface alloys on an aluminum substrate by a high-current pulsed electron beam. A multilayer system Al/Si/Al/Si/Al/Si/Al was deposited on an Al substrate using a physical vapor deposition (PVD) technique. The multilayer system consists of four polycrystalline Al films with a thickness of 350 nm, divided by three amorphous-like 50-nm-thick Si films. An electron-beam surface alloying was realized where the technological conditions of the process led to a melting of the Al, but under the melting point of Si. Although the results revealed an unchanged multilayer structure after the electron-beam alloying, the concentration of the silicon in the Al layers was significantly increased, due to the diffusion of the Si atoms within the Al films. The following rapid solidification of Si-rich Al layers led to the formation of a second-phase structure of $Al_4Si_2C_5$. With an increase in the beam energy, where the melting point of Si was reached, the effectiveness of the element mixing significantly decreased due to the ablation of the deposited multilayer system. Concerning the formation of Al–C surface alloys, a multilayer system of Al/C/Al/C was deposited on Al substrate by PVD technology. The multilayer film consists of two polycrystalline Al films with thicknesses of 700 nm and 500 nm and two amorphous-like C with thicknesses of 200 nm and 100 nm. The electron-beam alloying process was realized in the mode of melting of Al and the resultant structure consists of coarse unmelted Al particles, regions consisted of nanosized (2–3 nm) C particles located at the grain boundaries of submicron Al grains, zones consisted of 50–100 nm carbon structures with 3–5 nm Al precipitates, as well as few micrometers amorphous-like

carbon particles. In comparison with the previous system (Al–Si), second phase structures have not been observed due to the low temperature and short lifetime of the melt pool [50–52].

Similarly, Zhang et al. [55] have studied an alloying of Al substrate with Cr powders by a high-current pulsed electron beam. The results obtained in this work showed that the Al–Cr-alloyed layer was successfully formed using electron-beam alloying, and surface properties of the base Al material were significantly improved. It was found that Al_8Cr_5, $AlCr_2$ and $Al_{13}Cr_2$ intermetallics, as well as ultrafine Cr particles and Al(Cr) solid solutions were obtained within the alloyed zone. The microhardness was significantly increased, and the corrosion properties were greatly improved over the Al substrate.

The authors of [49,53,54] have based their work on electron-beam-alloying of aluminum alloys with Fe, Cr, Co and Ni powders. The alloying materials were previously deposited on the Al–Si substrate in the form of surface layers with a thickness of 1 μm. The obtained results showed that the alloying of Al–Si alloy with Fe–Cr powders led to a formation of $FeSiAl_6$; Al_3Fe; $CrAl_7$; $(CrFe)_4Si_4Al_{13}$; $(CrFe)_5Si_8Al_2$ phases and up to 8.4% Fe solid solutions. Concerning the alloying with Ni–Cr powders, the following phases were registered: $NiAl_3$, Cu_4NiAl_7 and $(CuFeNi)_2Al_3$. At very high cooling rates, supersaturated solid solutions with a chromium content of up to 10% were formed. The alloying of Al–Si material with Co–Cr powders led to a formation of Co_2Al_9 and $CoCu_2Al_7$. It was found that the microhardness of the alloyed zone in all cases was significantly higher than the base Al–Si material, where the highest values were found in the case of alloying with Co–Cr powders (about 240 HV).

The authors of [56,57] studied the possibility of formation of ternary Al–Ti–Nb surface alloys by electron-beam alloying of Al substrate with Ti and Nb films, where the influence of the speed of the specimen motion on the structure and properties of the intermetallics was investigated. The results showed a presence of pseudobinary $(Ti,Nb)Al_3$ intermetallic phase, and the velocity of the sample movement did not influence on the phase composition. The measured microhardness of the intermetallic phase reached 775 HV, which is about 22 times higher than the base Al substrate. It was found that the speed of the specimen motion has a significant influence on the microstructure. In the case of higher velocity, the microstructure of the alloyed zone consists of fine intermetallic particles, homogeneously distributed on the surface of the Al substrate with a very small amount of coarse fractions, while at a lower speed it is in the form of coarse intermetallic fractions (Figure 9). The same authors [56] have made an extensive discussion on the influence of the speed motion on the resultant microstructure and the distribution of the alloying elements within the surface alloys formed by electron-beam alloying. According to the numeric model [58], which studied the mass transport in the melt pool, the homogenization of surface alloys formed by high energy fluxes is based on the high-temperature Marangoni convection, caused by the high-temperature gradient in the molten material. The influence of the convection on the homogenization can be evaluated by the surface tension number S, which is given by Equation (7):

$$S = \frac{\left(\frac{d\sigma}{dT}\right)qd}{\mu u_0 k} \quad (7)$$

In (7) $(d\sigma/dT)$—temperature coefficient of the surface tension; q—net heat flow; d—electron beam diameter; μ—viscosity; u_0—the speed of the sample motion; k—thermal conductivity. For lower values of the surface tension number, the mass transport is insufficient for melt homogenization due to the negligible convection processes, and vice versa. On the other hand, it is evident from (7) that the use of the lower speed of sample motion during the alloying process leads to higher values of S and the convection is sufficiently intensive for melt-homogenization and causing solute redistribution. These statements are completely in agreement with the results obtained by the authors of [56,57], where it was demonstrated that lower velocity of sample movement leads to a formation of significantly more homogeneous microstructure than higher speeds (Figure 10).

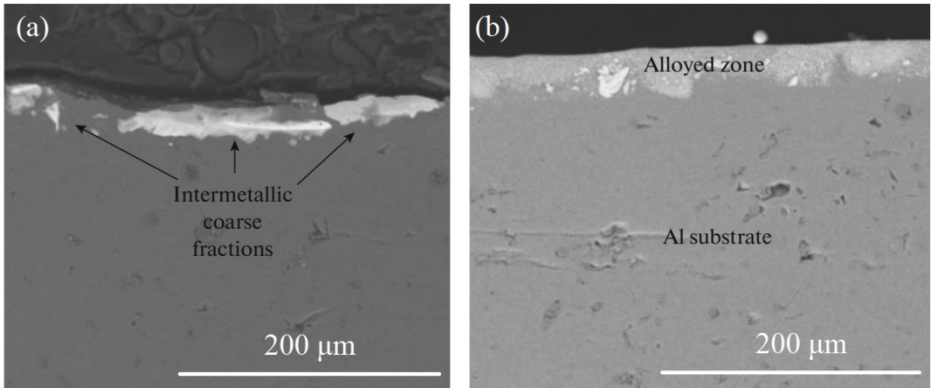

Figure 10. Cross-sectional SEM images of Al–Ti–Nb surface alloys, formed by electron-beam surface alloying with (**a**) higher and (**b**) lower speed of specimen motion [57]. (Reproduced with permission from ref. [57]. Copyright (2018), Springer Nature).

5.2. Electron-Beam Surface Alloying of Titanium and Its Alloys

There exist many works which describe the alloying of titanium and Ti-based alloys by electron-beam techniques [50,59–66]. The authors of [59,60] have studied the possibilities of alloying of the Ti substrate with Al film by electron-beam alloying. The thickness of the deposited Al film was 100 nm. The specimens were then subjected to electron-beam surface alloying. The results showed that a surface alloy with a thickness of 2 μm was successfully formed. The concentration of the Al element decreases with an increase in the depth of the sample. The phase composition consists of TiAl ($TiAl_2$), Ti_3Al and α-Ti, where TiAl ($TiAl_2$) was the main one and was replaced by Ti_3Al and α-Ti in the deeper parts of the specimen. The results showed that the microhardness of the obtained surface alloy was 11 GPa on the surface and decreases with an increase in the depth. Similarly, the authors of [61] studied an alloying of the Ti substrate with a composite Ti–Al (Ti:Al = 1:1) film by electron-beam surface alloying. The phase composition consists of TiAl/Ti_3Al phases, and it was demonstrated that the hardness was 18.5 GPa on the surface and decreases to about 5 GPa at a depth of 1500 nm.

The authors of [50,62,63] studied the possibilities of electron-beam surface alloying of Ti-6Al-4V alloy with Zr and Ti. A multilayer Zr/Ti coating with a thickness of 480 nm was deposited on the Ti-6Al-4V substrate by DC (direct current) magnetron sputtering. The specimens were then electron-beam surface alloyed, which led to a homogeneous mixing of the Ti–Zr films, and the diffusion of Zr within the Ti-6Al-4V substrate—up to a thickness of 1 μm. The performed EDS analysis showed an absence of Al and V atoms up to a depth of 500 nm. The XRD results demonstrated the presence of the $Ti_{70}Zr_{40}$ phase. Similarly, Zhang et al. [64] studied an alloying of Ti-6Al-4V substrates with Cr powder by a high-current pulsed electron beam. The results obtained by the authors of [64] showed that the microstructure of the formed surface alloy was transformed from $\alpha + \beta$ structure to α' laths and β equiaxed grains. Additionally, uniformly distributed Cr_2Ti particles were also observed within the alloyed layer. It was found that the hardness of the surface alloy was increased with an increase in the number of pulses. The hardness of the initial sample was found to be 298 HV and reaches values of 362 HV for the Cr-alloyed specimen, irradiated with 30 pulses. Moreover, a significant improvement was reported for the coefficient of friction and wear properties. Both, the friction coefficient and wear rate decreased gradually with an increase in the number of the pulses. In addition, it was demonstrated that the corrosion properties of the Cr-alloyed Ti-6Al-4V specimen was the best after irradiation with 30 pulses [64].

The authors of [65] have shown the conditions of formation and characterization of Ti–Al–Nb and Ti–Al–V surface alloys on a Ti substrate by electron-beam alloying. Bilayer coatings of Ti-Nb and Ti-V respectively were deposited on a Ti substrate by DC (direct current) magnetron sputtering, in which the overall thickness of each coating was about 2 μm. The electron-beam current was varied in

the range from 15 mA to 25 mA with a step of 5 mA. The results showed that a surface alloy in the ternary system of Ti–Al–Nb was successfully obtained by using a beam current of 25 mA. However, although some amount of Al and Nb were successfully introduced into the Ti substrate, the presence of intermetallic phases in the system of Ti–Al–Nb was not registered. It was reported that the Al and Nb concentration within the alloyed zone was 8.9 at% and 6.0 at%, respectively. Lower values of the electron-beam current lead to insufficient input energy density and the Nb film remains unmelted (Figure 11). Concerning the formation of the Ti–Al–V surface alloys, it was demonstrated that it was successfully formed by a beam current of 20 mA. Higher values lead to the evaporation of the alloying elements (i.e., deposited Al–V bilayer coating) and the intermetallic has not been formed.

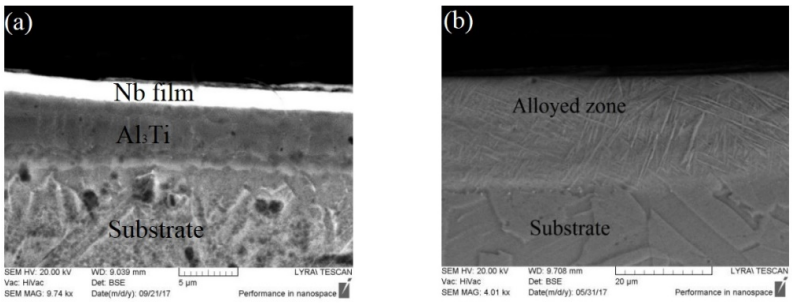

Figure 11. Cross-sectional SEM images of Ti–Al–Nb surface alloys, formed by electron-beam surface alloying with (**a**) electron-beam current of 20 mA (**b**) electron-beam current of 25 mA [65].

As already mentioned, the alloying of pure Ti substrate with Al and Nb by using a beam current of 25 mA led to a successful introduction of the alloying elements into the base material, but intermetallic phases within the discussed ternary system have not been observed. The same authors continued their research [66] by realizing a cyclic technique for the incorporation of the alloying elements into the Ti matrix. A scheme of the technique is presented in Figure 12. The maximum number of the realized cycles was three. The first was an electron-beam surface alloying of pure Ti substrate with a bilayer Al/Nb coating where the technological conditions of the alloying process were optimized according to [65]. The sample obtained after the first cycle was further covered by the same bilayer coating and subjected to a second electron-beam alloying. The same procedure was repeated for the third cycle. The results from [66] showed that the amount of the alloying elements increases after each cycle. After the second one, an intermetallic phase in the system of Ti–Al–Nb, namely body-centered cubic—B2 (BCC–B2) Ti_2AlNb was formed. After the third cycle, the phase composition was in the form of a double-phase structure of (BCC–B2) and orthorhombic (O) Ti_2AlNb. In addition, the results revealed that the microhardness increases after each cycle.

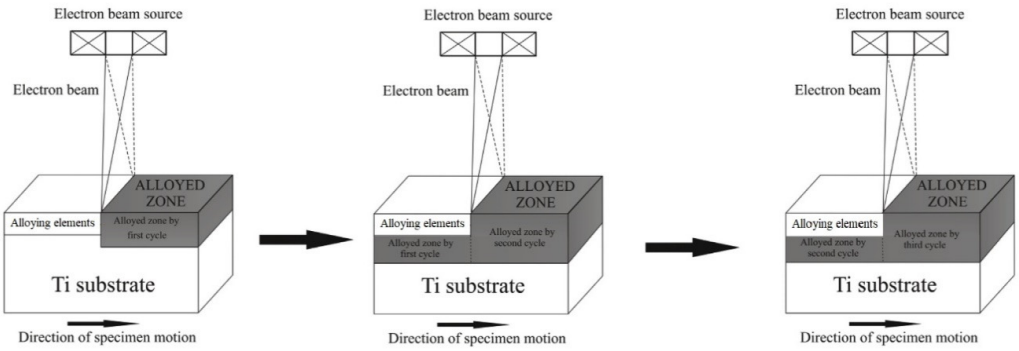

Figure 12. Scheme of cyclic electron-beam surface alloying of Ti substrate with Al/Nb bilayer coating [66]. (Reproduced with permission from ref. [66]. Copyright (2018), Elsevier).

5.3. Electron-Beam Surface Alloying of Other Materials

The authors of [67] studied an electron-beam surface alloying of stainless steel 316 with copper. A Cu film was deposited on the steel substrate by sputtering followed by a single pulsed melting of the film-substrate system. The results exhibited the best values for the nanohardness and wear resistance at an input energy density in the range from 4.3 to 6.3 J/cm^2. An increase in the pulse number to five at a constant input energy density led to a dissolution of the Cu film within the substrate and about 2 μm thick surface alloy was formed.

The authors of [68,69] studied an alloying of Ni substrates with W and Cr, respectively. In [68] an alloying of a commercially pure Ni with W powder using a high-current pulsed electron beam was studied. Two types of technological conditions were realized, namely 10 and 20 pulses. The results showed that the W powder was dissolved into the Ni substrate and formed a Ni(W) solid solution, Ni phase and ultrafine W particles. The microhardness and wear resistance increased with an increase in the number of pulses. These improvements were attributed mainly to the formed microstructural defects, the existence of W particles and Ni subgrains. In addition, the alloying process led to an enhancement in the corrosion properties due to induced microstructural defects and W additions, which led to the formation of a more stable passive film. Similarly, the authors of [69] studied the alloying of pure Ni with Cr powder, where two types of technological conditions were used: 10 and 20 pulses. The results showed that the hardness and wear resistance increased, and the coefficient of friction decreased with an increase in the pulse number. The corrosion resistance of the formed Ni–Cr surface alloy was also improved over the Ni substrate, where the best corrosion properties were found at the electron-beam alloying with 20 pulses. The authors of [70] investigated surface alloying of pure Ni substrates with chromium, tungsten and tin powders by pulsed electron beam and discuss the straightening mechanism. Their discussion was built on the first-principle calculations based on density functional theory. Two technological conditions were realized, namely 10 pulses and 20 pulses. The results showed that after 20 pulses of the electron-beam irradiation the amount of the alloying elements in the Ni matrix is greater than the alloying with 10 pulses. It was found that the Ni–Sn solid solution formed after 20 pulses has the highest microhardness. The same authors [70] discussed that the atomic radius is of major importance. They pointed out that the largest atomic radius of alloying elements led to the finest microstructure and highest hardness.

The authors of [71] studied alloying Cu substrates with W powder by a high-current pulsed electron beam. The alloying procedure was carried out at 20 and 30 pulses and the results revealed that the highest value of the hardness (38% greater than unalloyed specimen) and enhancement of the corrosion properties were obtained after alloying with 30 pulses. The same authors extended their research by comparison of high-current pulsed electron-beam alloying of Cu–Cr and Cu–W under the same technological conditions [72]. It was found that the Cu–Cr solid solution exhibits significantly higher hardness than that of Cu–W. The reason was the existence of deformation structures, subgrains, solid solution and Cr particles. The same authors mentioned that the particle-strengthening mechanism is of major importance for the microhardness enhancement of the Cu matrix.

Based on the performed literature review, it is obvious that the electron-beam alloying technique has many applications in the field of improving the surface properties of a wide range of materials. Comparing the enhancement of the surface properties of Ti, Al and its alloys by electron-beam hardening vs alloying, the first approach leads to an increase in the hardness in the range from 20% to 40%, while the latter one is capable in increasing the mechanical properties to more than 20 times [56]. The electron-beam alloying technology is significantly more appropriate for the improvement of the surface properties of light metals and alloys in comparison to the other electron-beam treatment techniques.

6. Summary

The techniques and trends of electron-beam surface treatment of metals and alloys—including hardening, alloying and electron-beam physical vapor deposition—were presented in this article.

Some combined methods and techniques for improvement of the structure and properties of advanced materials were also discussed. The major benefits of these techniques are their low cost, short process time, repeatability of the technological conditions. It was shown that the electron-beam treatment technologies lead to a significant improvement in the functional properties of different metals and alloys and can be applied in a number of modern industrial branches, such as aerospace, automotive, marine industries, aircraft manufacturing, biomedical applications, etc. This improvement is mostly due to grain refinement, phase transformations, changes in the microstructure, caused by the high cooling rates. The data related to the functional properties of many materials, such as aluminum, titanium, stainless steels, tool steels were presented and extensively discussed. The results showed that their characteristics were significantly improved, from about 20% to more than 20 times, which significantly exceed that obtained by the conventional techniques.

Currently, many researchers have based their work on the optimization of the technological conditions, structure and properties of electron-beam processed materials—as well as for their implementation in completely new industrial fields. Due to the fact that many electron-beam machines are already installed in many industrial factories and their number growths rapidly every year, the usage of these technologies in the modern industry will grow further. It can be concluded that the electron-beam methods for surface treatment are very promising and their industrial applications still growing.

Author Contributions: Conceptualization, S.V., M.O. and P.P.; writing—original draft preparation, S.V. and M.O.; writing—review and editing, P.P. All authors have read and agreed to the published version of the manuscript.

Funding: This research was funded by the Bulgarian National Science Fund; Grant Number KP-06-M37/5.

Conflicts of Interest: The authors declare no conflict of interest.

References

1. Yusuf, S.; Cutler, S.; Gao, N. Review: The Impact of Metal Additive Manufacturing on the Aerospace Industry. *Metals* **2019**, *9*, 1286. [CrossRef]
2. Portoles, L.; Jorda, O.; Jorda, L.; Uriondo, A.; Esperson-Miguez, M.; Perinpanayagam, S. A qualification procedure to manufacture and repair aerospace parts with electron beam melting. *J. Manuf. Syst.* **2016**, *41*, 65–75. [CrossRef]
3. Juechter, V.; Franke, M.; Merenda, T.; Stich, A.; Korner, C.; Singer, R. Additive manufacturing of Ti-45Al-4Nb-C by selective electron beam melting for automotive applications. *Addit. Manuf.* **2018**, *22*, 118–126. [CrossRef]
4. Murr, L.; Gaytan, S.; Ceytan, A.; Martinez, E.; Martinez, J.; Hernandez, D.; Machado, B.; Ramirez, D.; Medina, F.; Collins, S.; et al. Characterization of titanium aluminide alloy components fabricated by additive manufacturing using electron beam melting. *Acta Mater.* **2010**, *58*, 1887–1894. [CrossRef]
5. Weglowski, M. Electron beam rapid prototyping using wires and modification of the surface. In *Manufacturing Techniques for Materials: Engineering and Engineered*, 1st ed.; Srivatsan, T., Sudarshan, T., Manigandan, K., Eds.; Taylor and Francis Group: Boca Raton, FL, USA, 2018; pp. 133–160.
6. Weglowski, M.; Blacha, S.; Philips, A. Electron beam welding-Techniques and trends-Review. *Vacuum* **2016**, *130*, 72–92. [CrossRef]
7. Abroyan, I.; Andronov, A.; Titov, A. *Physical Fundamentals of Electron and Ion Technology*; Vysshaya Shkola: Moscow, Russia, 1984. (In Russian)
8. Schultz, H. *Electron Beam Welding*; Abington Publishing: Cambridge, UK, 1993.
9. Petrov, P.; Tongov, M. Numerical modelling of heat source during electron beam welding. *Vacuum* **2020**, *171*, 108991. [CrossRef]
10. Kaisheva, D.; Angelov, V.; Petrov, P. Simulation of heat transfer at welding with oscillating electron beam. *Can. J. Phys.* **2019**, *97*, 1140–1146. [CrossRef]
11. Bishop, C. *Electron Beam (E-beam) Evaporation, In Vacuum Deposition onto Webs, Films and Foils*; William Andrew: Norwich, NY, USA, 2011; pp. 261–272.
12. Zou, J.; Qin, Y.; Dong, C.; Wang, X.; Wu, A.; Hao, S. Numerical simulation of the thermal-mechanical process of high current pulsed electron beam treatment. *J. Vac. Sci. Technol. A* **2004**, *22*, 545–552. [CrossRef]

13. Proskurovsky, D.; Rotshtein, V.; Ozur, G.; Markov, A.; Nazarov, D.S. Pulsed electron-beam technology for surface modification of metallic materials. *J. Vac. Sci. Technol. A* **1998**, *16*, 2480–2488. [CrossRef]
14. Panin, A.; Kazachenok, M.; Perevalova, O.; Martynov, S.; Panina, A.; Sklyarova, E. Continuous Electron Beam Post-Treatment of EBF^3-Fabricated Ti–6Al–4V Parts. *Metals* **2019**, *9*, 699. [CrossRef]
15. Bocharov, A.; Murygin, A.; Laptenok, V. Calculating the geometric parameters of the distribution of electron beam energy density on its section in EBW. *IOP Conf. Ser. Mater. Sci. Eng.* **2018**, *450*, 032010. [CrossRef]
16. Bohm, S. *The Electron Beam as a Tool for Joining Technology*; DVS Media GmbH: Düsseldorf, Germany, 2014; pp. 1–100.
17. Klimpel, A. *Welding Handbook*; Silesian University of Technology: Gliwice, Poland, 2013; Volume 1, pp. 601–654.
18. Angelov, V.; Ormanova, M.; Kaisheva, D.; Lazarova, R.; Dimitrova, R.; Petrov, P. Selective electron beam surface alloying of aluminum with TiCN nanoparticles. *Nucl. Instrum. Methods Phys. Res. B* **2019**, *440*, 88–94. [CrossRef]
19. Valkov, S.; Ormanova, M.; Petrov, P. Surface manufacturing of materials by high energy fluxes. In *Advanced Surface Engineering Research*; Chowdhury, M.A., Ed.; IntechOpen: London, UK, 2018; pp. 69–87.
20. Schiller, S.; Heisig, U.; Panzer, S. *Electron Beam Technology*; Willey: Hoboken, NJ, USA, 1982; p. 508.
21. Farrahi, G.; Sistaninia, M. Thermal analysis of laser hardening for different moving patterns. *IJE Trans. A Basics* **2009**, *22*, 169–180.
22. Ormanova, M.; Angelov, V.; Petrov, P. Investigation of thermal processes at electron-beam surface modification by means of scanning electron beam. *J. Phys. Conf. Ser.* **2016**, *700*, 012033. [CrossRef]
23. Beck, J.; Cole, K.; Haji-Sheikh, A.; Litkouhi, B. *Heat Conduction Using Greens Functions*, 2nd ed.; Taylor & Francis: Oxfordshire, UK, 2011.
24. Kaisheva, D. A Study of the Physical Processes at Welding of Materials by High Energy Fluxes. Ph.D. Thesis, Institute of Electronics, Bulgarian Academy of Sciences, Sofia, Bulgaria, 2020.
25. Zenker, R. Modern thermal electron beam processes—Research results and industrial application. *La Metall. Ital.* **2009**, *101*, 1–8.
26. Dossett, J.; Totten, G. ASM Handbook. In *Steel Heat Treating Fundamentals and Processes*; ASM International: New York, NY, USA, 2013; Volume 4A.
27. Wei, D.; Wang, X.; Wang, R.; Cui, H. Surface modification of 5CrMnMo steel with continuous scanning electron beam process. *Vacuum* **2018**, *149*, 118–123. [CrossRef]
28. Fu, Y.; Hu, J.; Shen, X.; Wang, Y.; Zhao, W. Surface hardening of 30CrMnSiA steel using continuous electron beam. *Nucl. Instrum. Methods Phys. Res. B* **2017**, *410*, 207–214. [CrossRef]
29. Petrov, P. Optimization of carbon steel electron-beam hardening. *J. Phys. Conf. Ser.* **2010**, *223*, 012029. [CrossRef]
30. Petrov, P.; Dimitrov, D.; Aprakova, M.; Valkanov, S. Surface Hardening of Alloy Steels Using a High Intensity Electron Beam. *Mater. Manuf. Process.* **1998**, *13*, 555–564. [CrossRef]
31. Zenker, R.; Buchwalder, A. *Elektronenstrahl Randschichtbehandlung: Innovative Technologien für höchste industrielle Ansprüche*; Pro-beam AG & Co. KGaA: Gilching, Germany, 2010; pp. 1–89.
32. Song, R.; Zhang, K.; Chen, G. Electron beam surface treatment. Part I: Surface hardening of AISI D3 tool steel. *Vacuum* **2003**, *69*, 513–516. [CrossRef]
33. Gao, Y. Surface modification of TA2 pure titanium by low energy high current pulsed electron beam treatments. *Appl. Surf. Sci.* **2011**, *257*, 7455–7460. [CrossRef]
34. Gao, Y. Influence of pulsed electron beam treatment on microstructure and properties of TA15 titanium alloy. *Appl. Surf. Sci.* **2013**, *264*, 633–635. [CrossRef]
35. Ramskogler, C.; Warchomicka, F.; Mostofi, S.; Weinberg, A.; Sommitsch, C. Innovative surface modification of Ti6Al4V alloy by electron beam technique for biomedical application. *Mater. Sci. Eng. C* **2017**, *78*, 105–113. [CrossRef] [PubMed]
36. Nikolova, M.; Yankov, E.; Petrov, P.; Valkov, S.; Ormanova, M.; Zaharieva, V.; Tonev, D.; Andreeva, A. Electron beam surface modification of Ti5Al4V alloy for biomedical applications. In Proceedings of the METAL 2017—26th International Conference on Metallurgy and Materials, Brno, Czech Republic, 24–26 May 2017; pp. 1555–1560.
37. Zagulyaev, D.; Konovalov, S.; Gromov, V.; Glezer, A.; Ivanov, Y.; Sundeev, R. Structure and properties changes of Al-Si alloy treated by pulsed electron beam. *Mater. Lett.* **2018**, *229*, 377–380. [CrossRef]

38. Mohandas, T.; Banerjee, D.; Kutumba Rao, V. Fusion zone microstructure and porosity in electron beam welds of an α+β titanium alloy. *Metall. Mater. Trans. A* **1990**, *30A*, 789–798.
39. Dimitrov, D.; Aprakova, M.; Valkanov, S.; Petrov, P. Electron beam hardening of ion nitrided layers. *Vacuum* **1998**, *49*, 239–246. [CrossRef]
40. Zenker, R. Electron meets nitrogen: Combination of electron beam hardening and nitriding. *Int. Heat Treat. Surf. Eng.* **2009**, *3*, 141–146. [CrossRef]
41. Ormanova, M.; Petrov, P.; Kovacheva, D. Electron beam surface treatment of tool steels. *Vacuum* **2017**, *135*, 7–12. [CrossRef]
42. Grumbt, G.; Zenker, R.; Spies, H.; Franke, R.; Haase, I. Improvement of the wear behaviour of highly-loaded components and tools by multi-combined surface treatment. *Mater. Eng.* **2014**, *21*, 1–10.
43. Ormanova, M.; Dechev, D.; Bezdushnyi, R.; Petrov, P. Phase composition of multilayer system TiN/CrN deposited by DC magnetron sputtering. *Bulg. Chem. Commun.* **2017**, *49*, 98–102.
44. Petrov, P.; Dechev, D.; Ivanov, N.; Hikov, T.; Valkov, S.; Nikolova, M.; Yankov, E.; Parshorov, S.; Bezdushnyi, R.; Andreeva, A. Study of the influence of electron beam treatment of Ti5Al4V substrate on the mechanical properties and surface topography of multilayer TiN/TiO_2 coatings. *Vacuum* **2018**, *154*, 264–271. [CrossRef]
45. Valkov, S.; Parshorov, S.; Andreeva, A.; Bezdushnyi, R.; Nikolova, M.; Dechev, D.; Ivanov, N.; Petrov, P. Influence of Electron Beam Treatment of Co–Cr Alloy on the Growing Mechanism, Surface Topography, and Mechanical Properties of Deposited TiN/TiO_2 Coatings. *Coatings* **2019**, *9*, 513. [CrossRef]
46. Grumbt, G.; Zenker, R.; Biermann, H.; Weigel, K.; Bewilogua, K.; Bräuer, G. Duplex Surface Treatment—Physical Vapor Deposition (PVD) and Subsequent Electron Beam Hardening (EBH). *Adv. Eng. Mater.* **2014**, *16*, 511–516. [CrossRef]
47. Zaguliaev, D.; Gromov, V.; Rubannikova, Y.; Konovalov, S.; Ivanov, Y.; Romanov, D.; Semin, A. Structure and phase states modification of AL-11SI-2CU alloy processed by ion-plasma jet and pulsed electron beam. *Surf. Coat. Technol.* **2020**, *383*, 125246. [CrossRef]
48. Zaguliaev, D.; Konovalov, S.; Ivanov, Y.; Gromov, V. Effect of electron-plasma alloying on structure and mechanical properties of Al-Si alloy. *Appl. Surf. Sci.* **2019**, *498*, 143767. [CrossRef]
49. Petrov, P. Electron beam surface remelting and alloying of aluminium alloys. *Vacuum* **1997**, *48*, 49–50. [CrossRef]
50. Rotshtein, V.; Shulov, A. Surface Modification and Alloying of Aluminum and Titanium Alloys with Low-Energy, High-Current Electron Beams. *J. Metall.* **2011**, *2011*, 673685. [CrossRef]
51. Rotshtein, V.; Markov, A.; Ivanov, Y. Surface treatment of materials with low-energy, high-current electron beam. In *Materials Surface Processing by Directed Energy Techniques*; Pauleau, Y., Ed.; Elsevier: Amsterdam, The Netherlands, 2006; pp. 205–240.
52. Proskurovsky, D.; Rotshtein, V.; Ozur, G.; Ivanov, Y.; Markov, A. Physical foundations for surface treatment of materials with low energy, high current electron beams. *Surf. Coat. Technol.* **2000**, *125*, 49–56. [CrossRef]
53. Petrov, P.; Dimitroff, D. Electron beam alloying of aluminum alloys. *Vacuum* **1993**, *44*, 857–861. [CrossRef]
54. Petrov, P. Surface modification of aluminium alloys using hybrid treatment techniques. *J. Phys. Conf. Ser.* **2012**, *356*, 012035. [CrossRef]
55. Zhang, C.; Lv, P.; Xia, H.; Yang, Z.; Konovalov, S.; Chen, X.; Guan, Q. The microstructure and properties of nanostructured Cr-Al alloying layer fabricated by high-current pulsed electron beam. *Vacuum* **2019**, *167*, 263–270. [CrossRef]
56. Valkov, S.; Petrov, P.; Lazarova, R.; Bezdushnyi, R.; Dechev, D. Formation and characterization of Al–Ti–Nb alloys by electron-beam surface alloying. *Appl. Surf. Sci.* **2016**, *389*, 768–774. [CrossRef]
57. Valkov, S.; Neov, D.; Bezdushnyi, R.; Beskrovnyi, A.; Kozlenko, D.; Petrov, P. Study of the Microstructure, Crystallographic Structure and Thermal Stability of Al–Ti–Nb Alloys Produced by Selective Electron Beam Alloying. *J. Surf. Investig. X-ray Synchrotron Neutron Tech.* **2018**, *12*, 436–441. [CrossRef]
58. Chan, C.; Mazumder, J.; Chen, M. A two-dimensional transient model for convection in laser melted pool. *Metall. Trans. A* **1984**, *15*, 2175–2184. [CrossRef]
59. Mei, X.; Fu, J.; Li, X.; Rotshtein, V.; Koval, N.; Ma, T. Surface alloying of Al films/Ti substrate based on high-current pulsed electron beams irradiation. *Rare Metals* **2014**, *33*, 155–160. [CrossRef]
60. Rotshtein, V.; Ivanov, Y.; Kolubaeva, Y.; Mei, X.; Markov, A.; Naiden, E.; Ozur, G.; Oskomov, K.; Popov, S.; Pryadko, E.; et al. Synthesis of Ti_3Al and TiAl based surface alloys by pulsed electron-beam melting of Al(film)/Ti(substrate) system. *Tech. Phys. Lett.* **2011**, *37*, 226–229. [CrossRef]

61. Valkov, S.; Neov, D.; Luytov, D.; Petrov, P. Neutron diffraction of titanium aluminides formed by continuous electron-beam treatment. *J. Phys. Conf. Ser.* **2016**, *700*, 012034. [CrossRef]
62. Batrakov, A.; Markov, A.; Ozur, G.; Proskurovsky, D.; Rotshtein, V. Surface alloying of metallic substrates with pre-deposited films through a pulsed electron-beam mixing. *Eur. Phys. J. Appl. Phys.* **2008**, *43*, 283–288. [CrossRef]
63. Rotshtein, V.; Markov, A.; Shevchenko, N.; Reuther, H.; Oskomov, K.; Shulov, V. Surface doping of VT6 alloy with zirconium by pulsed electron-beam mixing of predeposited multilayer Zr/Ti film. *Tech. Phys. Lett.* **2008**, *34*, 891–894. [CrossRef]
64. Zhang, L.; Peng, C.; Yao, X.; Guan, Q.; Lu, R. Surface alloying of Cr on Ti6Al4V alloy induced by high-current pulseelectron beam. *Surf. Coat. Technol.* **2019**, *370*, 288–297. [CrossRef]
65. Valkov, S.; Bezdushnyi, R.; Petrov, P. Study of the influence of vanadium and niobium on the structure of Ti-Al-V and Ti-Al-Nb alloys formed by selective electron beam alloying. *J. Phys. Conf. Ser.* **2018**, *992*, 012053. [CrossRef]
66. Valkov, S.; Bezdushnyi, R.; Petrov, P. Synthesis, structure and mechanical properties of Ti-Al-Nb coatings formed by electron beam additive technique. *Vacuum* **2018**, *156*, 140–145. [CrossRef]
67. Rotshtein, V.; Ivanov, Y.; Markov, A.; Proskurovsky, D.; Karlik, K.; Oskomov, K.; Uglov, B.; Kuleshov, A.; Novitskaya, M.; Dub, S.; et al. Surface alloying of stainless steel 316 with copper usingpulsed electron-beam melting of film–substrate system. *Surf. Coat. Technol.* **2006**, *200*, 6378–6383. [CrossRef]
68. Zhang, L.; Peng, C.; Shi, J.; Jin, Y.; Lu, R. Influence of high current pulsed electron beam on microstructure and properties of Ni–W alloy coatings. *J. Alloys Compd.* **2020**, *858*, 154460. [CrossRef]
69. Zhang, L.; Peng, C.; Guan, J.; Lv, P.; Guan, Q. Nanocrystalline Cr-Ni Alloying Layer Induced by High-Current Pulsed Electron Beam. *Nanomaterials* **2019**, *9*, 74. [CrossRef]
70. Zhang, L.; Peng, C.-T.; Shi, J.; Lu, R. Surface alloying of chromium/tungsten/stannum on pure nickel and theoretical analysis of strengthening mechanism. *Appl. Surf. Sci.* **2020**, *532*, 147477. [CrossRef]
71. Zhang, C.; Lv, P.; Cai, J.; Peng, C.-T.; Jin, Y.; Guan, Q. The microstructure and properties of tungsten alloying layer on copper by high-current pulse electron beam. *Appl. Surf. Sci.* **2017**, *422*, 582–590. [CrossRef]
72. Zhang, C.; Tian, N.; Li, L.; Yang, Z.; Lv, P.; Yunxue, J.; Zhu, H.; Guan, Q. The effect of high-current pulsed electron beam on phase formation and surface properties of chromium/copper system. *Vacuum* **2020**, *174*, 109222. [CrossRef]